

# Nanoscale

Accepted Manuscript



This is an *Accepted Manuscript*, which has been through the Royal Society of Chemistry peer review process and has been accepted for publication.

*Accepted Manuscripts* are published online shortly after acceptance, before technical editing, formatting and proof reading. Using this free service, authors can make their results available to the community, in citable form, before we publish the edited article. We will replace this *Accepted Manuscript* with the edited and formatted *Advance Article* as soon as it is available.

You can find more information about *Accepted Manuscripts* in the [Information for Authors](#).

Please note that technical editing may introduce minor changes to the text and/or graphics, which may alter content. The journal's standard [Terms & Conditions](#) and the [Ethical guidelines](#) still apply. In no event shall the Royal Society of Chemistry be held responsible for any errors or omissions in this *Accepted Manuscript* or any consequences arising from the use of any information it contains.

Cite this: DOI: 10.1039/c0xx00000x

www.rsc.org/xxxxxx

**COMMUNICATION****DNA Induced Intense Plasmonic Circular Dichroism of Highly Purified Gold Nanobipyramids**Wenjing Liu,<sup>a</sup> Di Liu,<sup>a</sup> Zhening Zhu,<sup>a</sup> Bing Han,<sup>a</sup> Yan Gao,<sup>\*a</sup> and Zhiyong Tang<sup>\*a</sup>

Received (in XXX, XXX) Xth XXXXXXXXX 20XX, Accepted Xth XXXXXXXXX 20XX

DOI: 10.1039/b000000x

We report a strong and reversible CD response through the assembly of helical DNA and Au nanobipyramids (Au NBPs). Compared with common spherical Au nanoparticles or anisotropic Au nanorods, highly purified Au NBPs possess more intense electromagnetic field and improved surface plasmon resonance. Thus, the assembly of DNA and Au NBPs exhibits obviously enhanced plasmonic CD response. When the plasmonic CD is used for DNA detection, it shows high sensitivity and good reproducibility.

DNA is a helical biomolecule with accurate and programmable configuration, which has been exhibiting potential applications in the fields of nanoelectronics, nanomaterials and optics.<sup>1-10</sup> Particularly, recent studies have revealed that the double helical DNA can induce generation of plasmonic circular dichroism (CD) of noble metal nanocrystals. This plasmonic CD response is attributed to the chiral current inside the noble metal nanoparticles (NPs), which is induced by the chiral dipole of molecules or macromolecules.<sup>11</sup> The conventional way of fabricating the plasmonic CD system is to couple the noble metal NPs with chiral molecules such as chiral ligands,<sup>12</sup> amino acids,<sup>13</sup> peptides<sup>14, 15</sup> and polymers<sup>16-18</sup>. Compared with these molecules, DNA has three major advantages: (1) The relatively rigid double helical strand of DNA provides large chiral dipole and results in more intense CD response;<sup>19</sup> (2) DNA is easily designable and may serve as a versatile platform to fabricate varying chiral structures;<sup>20, 21</sup> (3) DNA induced assemblies are highly reversible and can be tuned by altering the solution temperature or pH value.<sup>1</sup> Such advantages make DNA a promising candidate for construction of chiral nanomaterials with unexceptionally strong CD response.<sup>1, 20, 21</sup>

In addition to the chiral dipole of the helical DNA, the surface plasmon resonance (SPR) intensity of noble metal NPs is another important prerequisite to obtain strong plasmonic CD response.<sup>11</sup> The intense CD signal is highly desirable in negative refraction, superlens and chiral detection, because the enhanced optical activity corresponds to the improvement of the device performance.<sup>22-24</sup> Previous work has proved that, compared with spherical Au NPs, the anisotropic Au nanorods (NRs) with the intense electromagnetic field can generate much stronger CD signal.<sup>13, 16</sup> Interestingly enough, theoretical calculation further disclosed that many NPs of the unusual shapes like Au nanotriangles,<sup>25</sup> Au nanostars<sup>26</sup> and Ag or Au nanobipyramids

(Au NBPs)<sup>27-29</sup> possess even stronger SPR features than that of Au NRs, owing to the increased electromagnetic field originated from the sharp tips or the antenna effect. Unfortunately, general difficulty in accurate synthesis of the above unusual Au NPs, e.g., the low yield, poor shape control and unsatisfactory monodispersity, severely impedes their plasmonic applications. As an example, the typical product of Au NBPs always contains a large amount of impurities such as Au NRs and Au NPs.<sup>30-32</sup> And the yield of Au NBPs is still lower than 50 %, even though many methods have been attempted to optimize the synthesis process in recent years.<sup>33, 34</sup> Obviously, if a method can be developed to obtain the highly purified Au NBPs, the corresponding chiral noble metal assemblies with the intense CD signal would be expected.

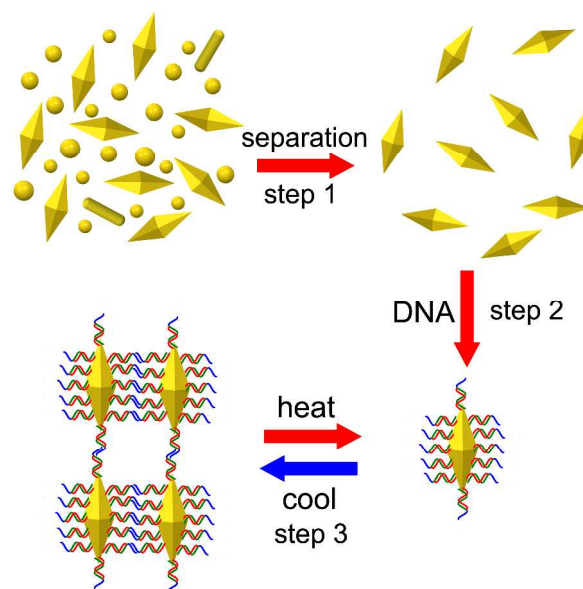


Fig. 1 A brief experimental procedure: Step 1, separation of as-synthesized Au NBPs; Step 2, modification of Au NBPs with helical DNA molecules; Step 3, dynamic assembly and intense CD response of Au NBPs.

In this work, density gradient centrifugation has been adopted to purify as-synthesized Au NBPs. Armed with the high yield of more than 90%, we report a strong and reversible CD response through the coupling between helical DNA molecules and Au NBPs. As illustrated in Fig. 1, a typical experimental procedure is

performed as follow: First, a separation method is used to improve the yield of the Au NBPs from 30% to 90 % (step 1 in Fig. 1). Subsequently, the helical DNA molecules are attached on the surface of Au NBPs via Au-S bond, and a weak CD signal appears (step 2 in Fig. 1). Finally, the complementary DNA chains are added to initiate the assembly of Au NBPs, and the CD response is enhanced for more than 11 times. Furthermore, the dynamic assembly of DNA and Au NBPs is manipulated reversibly with changing the solution temperature. Because of the strong SPR nature of Au NBPs, the CD response has a 7 times higher intensity than the previous reports based on the assembly of DNA and Au NRs.<sup>19</sup>

In a typical experiment, Au NBPs were synthesized by a seed-mediated method through reduction of Au<sup>3+</sup> ions (in the form of HAuCl<sub>4</sub>) onto the Au seed NPs.<sup>32</sup> As-prepared product was a mixture of Au NBPs, spherical Au NPs and a small amount of Au NRs. The yield of Au NBPs was no more than 30 %. It should be pointed out that though many efforts have been devoted to improve the synthesis process,<sup>26, 32, 35, 36</sup> the yield of Au NBPs is still below 65 %, which is far away from satisfying the application requirement. Herein, we focus on the simple separation of the Au NBPs from the crude product rather than the improvement of its yield by tedious synthesis routes.

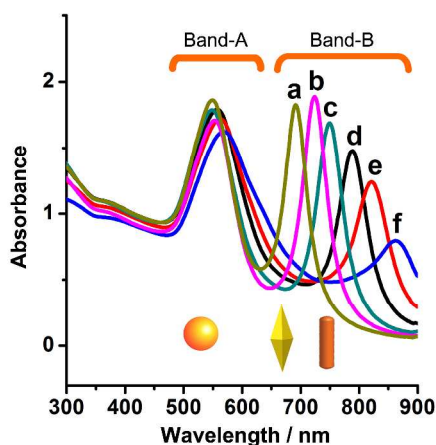


Fig. 2 UV-Vis absorption spectra of as-synthesized products containing Au NBPs, Au spherical NPs and Au NRs: from a to f, the LSPR of the products located at 692 nm, 724 nm, 750 nm, 789 nm, 821 nm, 862 nm, respectively.

The products containing Au NBPs of different aspect ratios are synthesized according to the previous report.<sup>32</sup> Typically, the crude products contain three different types of NPs including Au NBPs, spherical Au NPs and Au NRs. Two distinct bands are observed in the absorption spectra of as-prepared product: Band-A is located at ~550 to 570 nm while Band-B is spanned from 690 to 870 nm (Fig. 2). Band-A is mainly attributed to the absorbance characteristic of spherical Au NPs and the transverse SPR (TSPR) absorption of Au NBPs and Au NRs. Meanwhile, Band-B represents the longitudinal SPR (LSPR) absorption of one-dimensional (1D) Au NBPs and Au NRs. Because the content of Au NRs is very low in the crude products (typically less than 7 %), the yield of Au NBPs against the spherical Au NPs can be roughly estimated by the ratio of the Band-A to the Band-B. It is evident that with increase of the aspect ratio of Au

NBPs, the NBP tips become shaper, accompanying with red shift of the LSPR band from 690 to 870 nm (Figure S1, Table S1 and Figure S2). It is also noted that the yield of Au NBPs is gradually decreased as indicated from curves a to f in Fig. 2. Scanning electron microscopy (SEM) observations are consistent with the spectra results (Fig. S2).

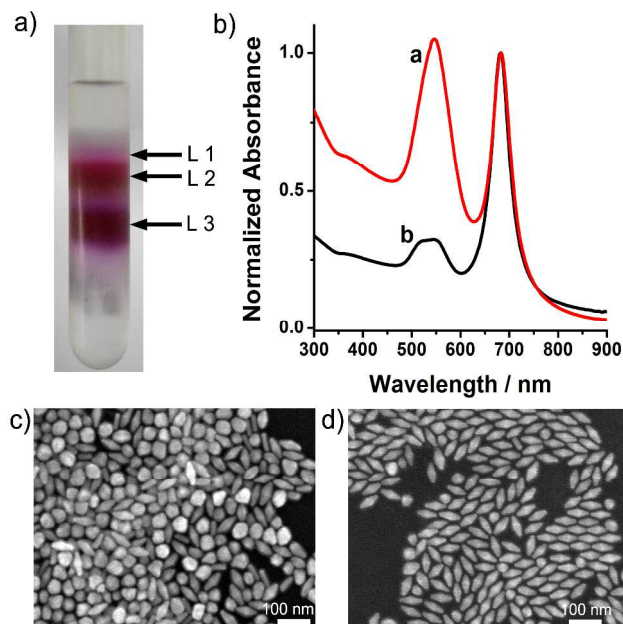


Fig. 3 Separation of Au NBPs in as-synthesized products: a) Digital image of separation of different Au NPs via density gradient centrifugation; b) UV-Vis absorption spectra of Au NBPs before (red curve) and after (black curve) purification; c) SEM image of the crude product; d) SEM image of Au NBPs after purification.

Thanks to the difference in shape and size of various Au NPs, density gradient centrifugation method can be utilized to purify the Au NBPs from as-synthesized products (see detailed experimental process in Supporting Information (SI)). As shown in Fig. 3a, after subjected to density gradient centrifugation, three clear layers appear in the centrifugation tube, corresponding to Au NRs, Au NBPs and Au NPs from L1 to L3, respectively (Fig. S3). By comparing the absorption spectra of Au NBPs before (red curve) and after (black curve) purification (Fig. 3b), one can easily recognize that the intensity of Band-A is tremendously decreased, indicating that most of the spherical Au NPs are removed from as-synthesized product. Significantly, in L2 of Fig. 3a, the yield of Au NBPs is increased from less than 30 % to more than 90 % (Fig. 3c and 3d). Moreover, the absorption line shape after density gradient centrifugation is well matched with the previous theoretical calculation about Au NBPs,<sup>27</sup> which confirms the high purity of Au NBPs in the separation product. It is worth mentioning that the LSPR peak of the purified Au NBPs possesses a very narrow full width at half-maximum (FWHM), about 50 nm (black curve in Fig. 3b), demonstrating a good monodispersity of the Au NBP product. Compared with Au NRs, narrower FWHM of Au NBPs would significantly benefit following optical detection for chiral molecules. And such highly purified Au NBPs lay a solid foundation for fabrication of the plasmonic assembly with helical DNA molecules of high

reproducibility and large optical activity.

To achieve the plasmonic CD response, the purified Au NBPs are firstly conjugated with single-strand DNA (SS-DNA) through the strong interaction between Au NBP surface and the mercapto end of DNA.<sup>6</sup> The SS-DNA used (sequence A) is presented as the red wavy lines in Fig. 1 with detailed sequence in SI. In addition, its complementary DNA (cDNA) (green wavy lines in Fig. 1) with sticky end of four extra bases (blue wavy lines in Fig. 1) is designed as sequence B (please see detailed sequence information in SI). After adding cDNA into the SS-DNA stabilized Au NBP solution, double-strand DNA (DS-DNA) modified Au NBPs would be produced. When the solution temperature (60 °C) is set above the melting temperature of DNA (50 °C), the individual DS-DNA modified Au NBPs are highly dispersed in the solution. Since DNA is a chiral molecule with distinct CD signals at UV region (Fig. S4), its chiral dipole can induce asymmetric electromagnetic field surrounding Au NBPs, resulting in a rather weak plasmonic peak at the visible light region (red curve in Fig. 4a). Furthermore, unlike the amino acid induced plasmonic CD response of Au NRs that exhibits a TSPR band at ~520 nm,<sup>13</sup> the CD peak corresponding to the TSPR band of Au NBPs at ~535 nm is absent (red curve in Fig. 4a). This observation can be understood that the TSPR of Au NBPs is much weaker than that of Au NRs,<sup>28</sup> giving rise to an undetectable electromagnetic coupling between the helical DNA and the TSPR band of Au NBPs. The difference in the plasmonic CD of the Au NBPs and Au NRs reveals that distribution of the SPR features surrounding noble metal NPs is significant for the resulted plasmonic CD response.

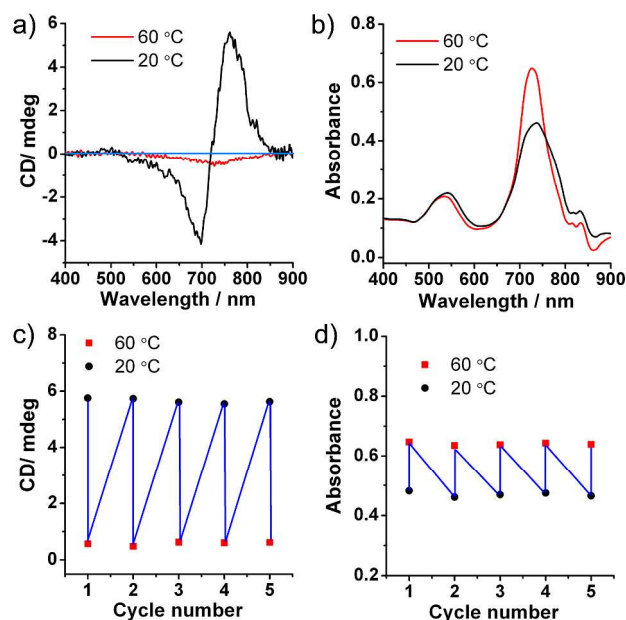


Fig. 4 a) CD and b) UV-Vis absorption spectra of DS-DNA modified Au NBPs at 20 °C (black curve) and 60 °C (red curve); temperature-dependent circle of c) CD intensity and d) absorption peak from 20 °C (black dot) to 60 °C (red dot).

More interestingly, when the solution temperature is decreased to 20 °C, the sticky end of cDNA could be complementary with each other, resulting in the self-assembly of Au NBPs (step 3 in Fig. 1). A typical property of the assembly recorded in the UV-

Vis absorption spectrum is the red shift of LSPR peak and the slight change of TSPR peak (black curve in Fig 4b).<sup>37</sup> Dynamic light scattering (DLS) measurement indicates the signal of Au NBPs is red-shifted because of the assembly (Fig. S5). After the spontaneous aggregation at 20 °C, the plasmonic CD response is obviously distinct from that of individual Au BPs at 60 °C: Not only is the CD intensity enhanced 11 times (5.76 at 762 nm vs. 0.52 at 729 nm), but also is the line shape split from single peak into doublet with opposite sign (black curve in Fig. 4a). With the assembly of Au NBPs, the LSPR coupling occurs, which greatly improves the intensity of the electromagnetic field surrounding the NPs *via* antenna effect and thus amplifies the plasmonic CD response. In addition, our recent study explored that the LSPR coupling of anisotropic Au NRs would cause energy splitting, resulting in the generation of two coupling modes (one is symmetric and the other is asymmetric) in the CD spectrum.<sup>13</sup> The Au NBPs have the similar morphology with Au NRs, so the bisignated CD peaks should be also attributed to the SPR coupling of the Au NBPs in the assembly. When the excited-state levels of the Au NBPs split into two levels via assembly, the lower energy level and the higher energy level correspond to two possible arrangements of the transition dipoles that are formed by the plasmon distribution in the dimer, respectively. As a result, an antibonding mode of higher energy and a bonding mode of lower energy are formed.

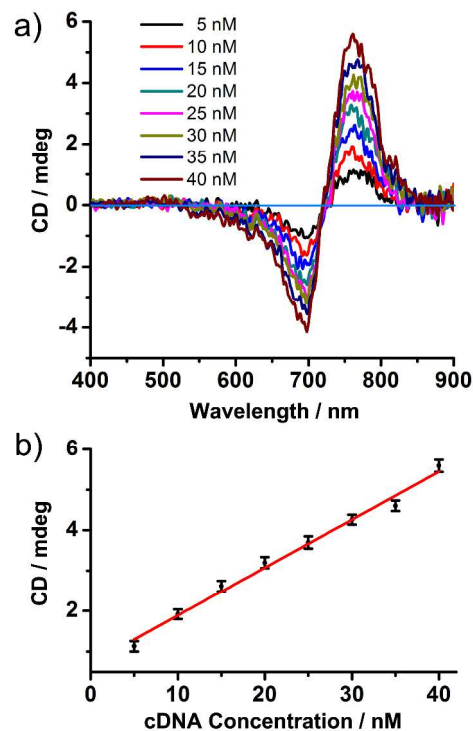


Fig. 5 a) CD spectra of Au NBP assemblies at 20 °C with varying concentration of cDNA (from 5 nM to 40 nM); b) standard analytical curve and the corresponding linear fitting ( $R^2 = 0.9883$ ).

Since the interaction of the sticky ends is a temperature-dependent process, one can easily manipulate the dynamic assembly of Au NBPs in a reversible way through the alternation of solution temperature (step 3 in Fig. 1). Five cycles of the

temperature change between 20 °C and 60 °C were performed, and the dynamic assembly process was monitored by both the CD and absorption spectrum (Fig 4c and 4d). During the temperature decrease, the plasmonic CD intensity is quickly changed from 5 ~0.52 to ~5.76. And as comparison, the change in the CD intensity is much more obvious than that in the absorption intensity (from 0.65 to 0.46), highlighting the advantage of plasmonic CD response of the anisotropic Au NPs in the field of highly sensitive detection.

10 Finally, we took advantage of the CD response of Au NBP assemblies at 20 °C to quantitatively measure the concentration of cDNA (Fig. 5). Evidently, higher concentration cDNA results in larger scale assembly of Au NBPs (Fig. S6), and thus generate stronger CD response (Fig. 5a). Without further rationalizing the 15 experimental parameters, the plasmonic CD signals (positive peak intensity at ~760 nm) exhibit a perfect linear relationship ( $R^2 = 0.9883$ ) with the concentration of cDNA varying from 5 nM to 40 nM (Fig. 5b), and the detection limit for cDNA is 5 nm. Such a bioanalysis based on the plasmonic response of Au NBP 20 assembly shows two major advantages. Compared with the minor intensity change in the UV-Vis absorption spectra from 0.55 to 0.45 (Fig. S6), the plasmonic CD intensity is more sensitive to the concentration of cDNA (from 1.13 to 5.58), making it promising for detection of helical DNA. We also notice that when the 25 concentration of cDNA is higher than 40 nM, the CD response remains unchanged (Fig. S7), likely because the saturate concentration of Sequence A on the surface of Au NBPs is about 40 nM. Another merit of Au NBP assembly is that the anisotropic factor (AF) of the CD response is up to  $4.36 \times 10^{-4}$  with 40 nM 30 cDNA added (red curve in upper spectra of Fig. 5); while in a similar method conducted by Au NRs, the AF is only  $1.21 \times 10^{-4}$  with 75 nM cDNA added. This result indicates that the Au NBP based plasmonic CD signal is about 7 times as that of Au NR assembly, which should be contributed by the intense 35 electromagnetic field and large LSPR intensity at the sharp tips of the Au NBPs.<sup>28</sup>

## Conclusions

In conclusion, we reported the plasmonic CD response of the highly purified Au NBPs induced by the helical DNA. Four key 40 parameters have been explored to contribute significantly to the intense CD response: 1) Purification of the Au NBPs (more than 90 %); 2) strong SPR feature of Au NBPs; 3) helical structure of DNA molecules; and 4) assembly of Au NBPs by DNA. Experimentally, we demonstrate that to use the noble metal NPs 45 with stronger SPR characteristics is an effective method to obtain enhanced plasmonic CD, remarkably benefiting highly sensitive detection of the helical structures or chiral molecules. The work will give us a new insight into achieving the giant optical activity with noble metal NPs of the specific geometries, which have 50 many potential applications in energy storage, metamaterials, circular polarizers and biosensors.<sup>38-46</sup>

## Acknowledgements

This work was partially supported by the National Key Basic Research Program of China (2014CB931801, Z.Y.T.), National 55 Natural Science Foundation for Distinguished Youth Scholars of

China (21025310, Z.Y.T.), National Natural Science Foundation of China (91027011, Z.Y.T.; 51272047, Y.G.).

## Notes and references

<sup>a</sup> Laboratory of Nanomaterials, National Center for Nanoscience and Technology, Beiyitiao No.11, Zhongguancun, Beijing, P. R. China. E-mail: gaoyan@nanoctr.cn, zytang@nanoctr.cn.

† Electronic Supplementary Information (ESI) available: [Detailed experimental procedure; additional CD and UV-Vis spectra, SEM images, DLS results]. See DOI: 10.1039/b000000x/

- 65 1. A. Kuzyk, R. Schreiber, Z. Y. Fan, G. Pardatscher, E. M. Roller, A. Hogele, F. C. Simmel, A. O. Govorov and T. Liedl, *Nature*, 2012, **483**, 311-314.
2. J. Sharma, R. Chhabra, A. Cheng, J. Brownell, Y. Liu and H. Yan, *Science*, 2009, **323**, 112-116.
- 70 3. L. B. Wang, L. G. Xu, H. Kuang, C. L. Xu and N. A. Kotov, *Acc. Chem Res*, 2012, **45**, 1916-1926.
4. D. Nykypanchuk, M. M. Maye, D. van der Lelie and O. Gang, *Nature*, 2008, **451**, 549-552.
5. W. L. Cheng, M. J. Campolongo, J. J. Cha, S. J. Tan, C. C. Umbach, D. A. Muller and D. Luo, *Nat. Mater.*, 2009, **8**, 519-525.
- 75 6. M. R. Jones, R. J. Macfarlane, B. Lee, J. A. Zhang, K. L. Young, A. J. Senesi and C. A. Mirkin, *Nat. Mater.*, 2010, **9**, 913-917.
7. S. J. Tan, M. J. Campolongo, D. Luo and W. L. Cheng, *Nat Nanotechnol*, 2011, **6**, 268-276.
- 80 8. R. J. Macfarlane, B. Lee, M. R. Jones, N. Harris, G. C. Schatz and C. A. Mirkin, *Science*, 2011, **334**, 204-208.
9. Z. T. Li, E. J. Cheng, W. X. Huang, T. Zhang, Z. Q. Yang, D. S. Liu and Z. Y. Tang, *J. Am. Chem. Soc.*, 2011, **133**, 15284-15287.
10. J. Sharma, R. Chhabra, C. S. Andersen, K. V. Gothelf, H. Yan and Y. Liu, *J. Am. Chem. Soc.*, 2008, **130**, 7820-7821.
- 85 11. A. O. Govorov, Z. Y. Fan, P. Hernandez, J. M. Slocik and R. R. Naik, *Nano Lett.*, 2010, **10**, 1374-1382.
12. X. Vidal, W. J. Kim, A. Baev, V. Tokar, H. Jee, M. T. Swihart and P. N. Prasad, *Nanoscale*, 2013, **5**, 10550-10555.
- 90 13. Z. N. Zhu, W. J. Liu, Z. T. Li, B. Han, Y. L. Zhou, Y. Gao and Z. Y. Tang, *Acs Nano*, 2012, **6**, 2326-2332.
14. Y. H. Xia, Y. L. Zhou and Z. Y. Tang, *Nanoscale*, 2011, **3**, 1374-1382.
15. J. M. Slocik, A. O. Govorov and R. R. Naik, *Nano Lett.*, 2011, **11**, 701-705.
- 95 16. A. Guerrero-Martinez, B. Auguie, J. L. Alonso-Gomez, Z. Dzolic, S. Gomez-Grana, M. Zinic, M. M. Cid and L. M. Liz-Marzan, *Angew. Chem. Int. Ed.*, 2011, **50**, 5499-5503.
17. H. Q. Qi, H., K. E. Shopsowitz, W. Y. Hamad and M. J. MacLachlan, *J. Am. Chem. Soc.*, 2011, **133**, 3728-3731.
- 100 18. H. S. Oh, S. Liu, H. Jee, A. Baev, M. T. Swihart and P. N. Prasad, *J. Am. Chem. Soc.*, 2010, **132**, 17346-17348.
19. Z. T. Li, Z. N. Zhu, W. J. Liu, Y. L. Zhou, B. Han, Y. Gao and Z. Y. Tang, *J. Am. Chem. Soc.*, 2012, **134**, 3322-3325.
20. X. B. Shen, A. Asenjo-Garcia, Q. Liu, Q. Jiang, F. J. G. de Abajo, N. Liu and B. Q. Ding, *Nano Lett.*, 2013, **13**, 2128-2133.
- 105 21. W. J. Yan, L. G. Xu, C. L. Xu, W. Ma, H. Kuang, L. B. Wang and N. A. Kotov, *J. Am. Chem. Soc.*, 2012, **134**, 15114-15121.
22. N. Liu and H. Giessen, *Angew. Chem. Int. Edit.*, 2010, **49**, 9838-9852.
23. W. J. Liu, Z. N. Zhu, K. Deng, Z. T. Li, Y. L. Zhou, H. B. Qu, Y. Gao, S. N. Che and Z. Y. Tang, *J. Am. Chem. Soc.*, 2013, **135**, 9659-9664.
- 110 24. B. Luk'yanchuk, N. I. Zheludev, S. A. Maier, N. J. Halas, P. Nordlander, H. Giessen and C. T. Chong, *Nat. Mater.*, 2010, **9**, 707-715.
25. D. A. Walker, K. P. Browne, B. Kowalczyk and B. A. Grzybowski, *Angew. Chem. Int. Ed.*, 2010, **49**, 6760-6763.
- 115 26. F. Hao, C. L. Nehl, J. H. Hafner and P. Nordlander, *Nano Lett.*, 2007, **7**, 729-732.
27. E. C. Le Ru, J. Grand, I. Sow, W. R. C. Somerville, P. G. Etchegoin, M. Treguer-Delapierre, G. Charron, N. Felidj, G. Levi and J. Aubard, *Nano Lett.*, 2011, **11**, 5013-5019.
- 120 28. A. Lombardi, M. Loumagne, A. Crut, P. Maioli, N. Del Fatti, F. Vallee, M. Spuch-Calvar, J. Burgin, J. Majimel and M. Treguer-Delapierre, *Langmuir*, 2012, **28**, 9027-9033.

29. J. Zhang, S. Li, J. Wu, G. C. Schatz and C. A. Mirkin, *Angew. Chem. Int. Edit.*, 2009, **48**, 7787-7791.
30. S. Lee, K. M. Mayer and J. H. Hafner, *Anal. Chem.*, 2009, **81**, 4450-4455.
- 5 31. M. Z. Liu and P. Guyot-Sionnest, *J. Phys. Chem. B*, 2005, **109**, 22192-22200.
32. X. S. Kou, S. Z. Zhang, C. K. Tsung, M. H. Yeung, Q. H. Shi, G. D. Stucky, L. D. Sun, J. F. Wang and C. H. Yan, *J. Phys. Chem. B*, 2006, **110**, 16377-16383.
- 10 33. X. S. Kou, W. H. Ni, C. K. Tsung, K. Chan, H. Q. Lin, G. D. Stucky and J. F. Wang, *Small*, 2007, **3**, 2103-2113.
34. H. Yoo and M. H. Jang, *Nanoscale*, 2013, **5**, 6708-6712.
35. H. Min-Chen, R. S. Liu and D. P. Tsai, *Cryst. Growth Des.*, 2009, **9**, 2079-2087.
- 15 36. J. Burgin, I. Florea, J. Majimel, A. Dobri, O. Ersenb and M. Tréguer-Delapierre, *Nanoscale*, 2012, **4**, 1299-1303.
37. P. K. Sudeep, S. T. S. Joseph and K. G. Thomas, *J. Am. Chem. Soc.*, 2005, **127**, 6516-6517.
38. Z. H. Nie, A. Petukhova and E. Kumacheva, *Nat. Nanotechnol.*, 2010, **5**, 15-25.
- 20 39. T. Wang, D. LaMontagne, J. Lynch, J. Q. Zhuang and Y. C. Cao, *Chem. Soc. Rev.*, 2013, **42**, 2804-2823.
40. J. H. Singh, G. Nair, A. Ghosh and A. Ghosh, *Nanoscale*, 2013, **5**, 7224-7228.
- 25 41. N. Abdulrahman, C. D. Syme, C. Jack, A. Karimullah, L. D. Barron, N. Gadegaard and M. Kadodwala, *Nanoscale*, 2013, **5**, 12651-12657.
42. Z. F. Huang, K. D. Harris and M. J. Brett, *Adv. Mater.*, 2009, **21**, 2983-2987.
43. S. H. Liu, Y. Y. Duan, X. J. Feng, J. Yang and S. A. Che, *Angew. Chem. Int. Ed.*, 2013, **52**, 6858-6862.
- 30 44. C. D. Sorrell and M. J. Serpe, *Adv. Mater.*, 2011, **23**, 4088-4092.
45. G. S. Lai, H. L. Zhang, J. W. Yong and A. M. Yu, *Biosens. Bioelectron.*, 2013, **47**, 178-183.
46. J. Hu, C. Wen, Z. Zhang, M. Xie, J. Hu, M. Wu and D. Pang, *Anal. Chem.*, 2013, **85**, 11929-11935.
- 35